KAPL-P-000046
(K96044)

CONF-960513--

CURRENT STATUS OF LOW-TEMPERATURE RADIATOR THERMOPHOTOVOLTAIC DEVICES

G.W. Charache, J.L. Egley, L.R. Danielson, D.M. DePoy, P.F. Baldasaro, B.C. Campbell, S. Hui. L.M. Frass. S.J. Wojtczuk

May1996

KAPL ATOMIC POWER LABORATORY   SCHENECTADY, NEW YORK 12301

Operated for the U. S. Department of Energy
by KAPL, Inc. a Lockheed Martin company

MASTER

DISCLAIMER

DISCLAIMER

Portions of this document may be illegible in electronic image products. Images are produced from the best available original document.

Current Status of Low-Temperature Radiator Thermophotovoltaic Devices

G.W. Charache, J.L. Egley, L.R. Danielson, D.M. DePoy, P.F. Baldasaro, and B.C. Campbell
Lockheed Martin Inc., Schenectady, NY 12301

S. Hui, and L.M. Fraas
JX-Crystals Inc. Issaquah, WA 98027

S.J. Wojtczuk
SPIRE Corp., Bedford, MA 01730

ABSTRACT

The current performance status of low-temperature radiator (< 1000 °C) thermophotovoltaic (TPV) devices is presented. For low-temperature radiators, both power density and efficiency are equally important in designing an effective TPV system. Comparisons of 1cm x 1cm, 0.55 eV InGaAs and InGaAsSb voltaic devices are presented. Currently, InGaAs lattice-mismatched devices offer superior performance in comparison to InGaAsSb lattice-matched devices, due to the former's long-term development for numerous optoelectronic applications. However, lattice-matched antimony-based quaternaries offer numerous potential advantages.

INTRODUCTION

Recently, low-temperature radiator (< 1000 °C) thermophotovoltaic (TPV) devices have been investigated by a number of laboratories [1,2]. This is in contrast to the large number of investigations carried out in the 1960s-1980s that concentrated on silicon or germanium TPV cells and high-temperature radiators (1500-2000 °C) [3]. Lowering the radiator temperature necessitates many changes in the design of TPV systems including development of low bandgap (0.4-0.7 eV) TPV devices and efficient below bandgap spectral control techniques (e.g., interference filter, plasma filter, metallic dipole filters, and back surface reflector). This paper presents a comparison of TPV diode performance for two competing low-bandgap materials ($E_g \cong 0.55$ eV): InGaAs and InGaAsSb. It must be noted that attaining high quality diodes is only one aspect of demonstrating a successful TPV device. The integration of an effective spectral control device is of equal importance for obtaining a high efficiency device.

InGaAs devices have been widely investigated for numerous high speed electronic and optoelectronic applications [4,5]. Over the bandgap range of interest, InGaAs is lattice mismatched to InP substrates; and therefore effective graded layers must be utilized to obtain high quantum efficiency and low dark current. This technology has been developed by a number of laboratories for TPV applications using primarily organometallic vapor-phase epitaxial (OMVPE) growth [1,2]. Due to this material system's relative maturity, the highest performance low bandgap TPV devices are currently InGaAs. Long-term reliability (>10^5 hours) at typical operating conditions (1-10A/cm^2, 50-100 °C) has yet to be determined for these lattice-mismatched devices.

Quaternary semiconductors allow independent variation of both bandgap and lattice constant. InGaAsSb is one potential semiconductor that can be grown lattice matched to either GaSb or InAs in the bandgap range of interest. This material system has recently been investigated for mid-IR (2-5 μm) quantum well lasers and detectors [6]. To date, liquid phase epitaxy (LPE) and molecular beam epitaxy (MBE) growth techniques have had the most success in obtaining high quality optoelectronic devices. However, OMVPE of InGaAsSb continues to be an active area of research [7]. LPE-grown devices on GaSb are limited to bandgaps of 0.53-0.7 eV due to the presence of a miscibility gap [8]. In addition to being lattice matched, advantages of this material system include: high hole mobility, simpler device structure, and tunneling reverse-bias breakdown which precludes the use of bypass diodes in high voltage arrays.

N-on-p InGaAs devices used for this comparison were fabricated at SPIRE Corp. using OMVPE, while p-on-n InGaAsSb devices were fabricated at JX-Crystals using LPE. Both devices were 1cm x 1cm; had a single 1-mm-wide central busbar; and utilized gridlines that were 10 μm-wide, 3-5 μm-thick, and spaced 100 μm apart. The InGaAs devices were grown in p$^+$-InP substrates and consisted of an ~4 μm-thick step-graded layer, a wide bandgap back surface field, an ~3 μm-thick p-base layer ($In_{0.72}Ga_{0.28}As$), a 0.25 μm-thick n$^+$-emitter layer, and a 0.02 μm-thick wide bandgap window layer [9]. InGaAsSb devices were grown on n-GaSb wafers and consisted of an ~10 μm-thick n-base layer and a diffused p$^+$ emitter.

EXPERIMENTAL RESULTS

Figure 1 illustrates typical quantum efficiency vs. wavelength for 0.54 eV InGaAs and 0.56 eV InGaAsSb TPV devices. This data was calibrated using a 0.55 eV device measured at NREL. Both devices show poor front surface recombination velocity as evidenced by the low quantum efficiency at short wavelengths. Thus, the window layer on the InGaAs device does not appear to be effective and needs improvement; while a window layer or passivation film on the InGaAsSb device should also lead to improved short wavelength quantum efficiency. The fall-off in quantum efficiency near the bandedge is believed to be due to a thin base in the case of InGaAs (i.e., photons not absorbed) and a thick base region in the case of InGaAsSb (i.e., ineffective back surface field). It is important to note that the long wavelength quantum efficiency is a larger contributor to overall current generation in low-temperature radiator TPV devices since the peak in photon flux corresponds to the bandedge of the TPV device active layers. Further modeling of accurate absorption coefficient data as a function of doping level and wavelength for these material systems is needed to verify these conclusions.
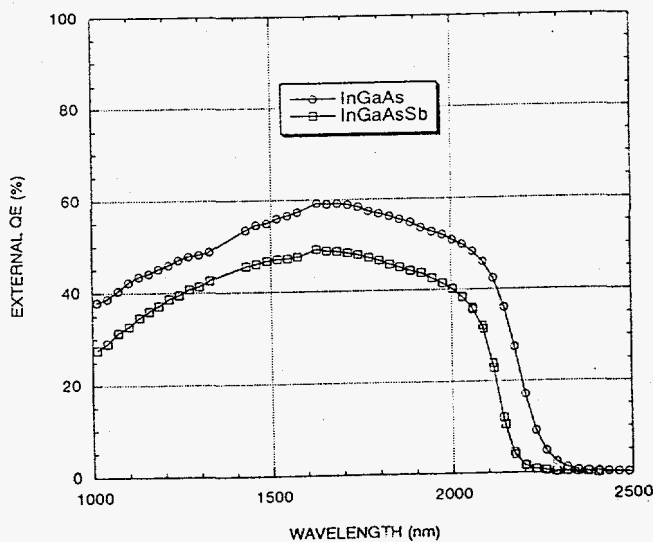

Figure 1 - Comparison of 0.54 eV InGaAs and 0.56 eV InGaAsSb TPV device quantum efficiency versus wavelength.

Figure 2 plots the measured short circuit current (I_{sc}) versus open circuit voltage (V_{oc}) for both InGaAs and InGaAsSb TPV devices. Neglecting shunt conduction, there are four potential dominant dark-current mechanisms: diffusion (n=1), bulk recombination/generation (n=2), surface recombination/generation (n=2) and band-to-band tunneling (n>2). Assuming a single dominant dark-current mechanism, the I_{sc} vs. V_{oc} data was fit to the following theoretical model:

$$I_{sc} \cong I_D \left(\exp\left(\frac{qV_{oc}}{nkT} \right) - 1 \right)$$

The InGaAs data has nearly ideal diffusion-limited behavior (n = 1.18) over the entire range of measured values. All n = 2 components are small. In contrast, the InGaAsSb device demonstrates n = 1.4 behavior at high short circuit currents and n > 2 behavior at low short circuit currents. Based on this data and subsequent temperature dependent measurements, the InGaAsSb dark current is believed to be tunneling limited at low current levels (n > 2), and recombination/generation (R-G) limited at high current levels (n = 2). It is suspected that Te-related bulk defects are causing the non-ideal behavior.
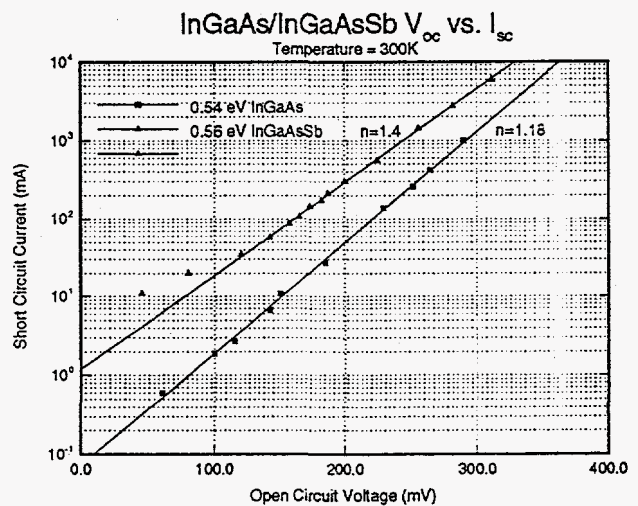

Figure 2 - Comparison of 0.54 eV InGaAs and 0.56 eV InGaAsSb TPV devices V_{oc} vs. I_{sc}.

Temperature-dependent illuminated current vs. voltage measurements were also taken to determine differences in the dominant dark-current mechanism. Samples were measured on a thermoelectrically-cooled chuck using separate current and voltage probes for both the front and back contacts (i.e., Kelvin probes). Figures 3 and 4 plot the measured open circuit versus temperature for the InGaAs and InGaAsSb devices, respectively, for different short circuit currents. In all cases the open circuit voltage decreases linearly with temperature over the measured temperature range. It was also noted that under fixed illumination, the short circuit current of both InGaAs and InGaAsSb increased slightly as the device temperature increased due to the bandedge shifting to longer wavelengths as expected. The 0.54 eV InGaAs has a V_{oc} temperature change of ~1.5 mV/°C, which is independent of current level. The 0.56 eV InGaAsSb has a V_{oc} temperature

dependence of ~1.45 mV/°C, which is independent of current level above 20 mA. Below this threshold, V_{oc} shows a much lower temperature dependence of ~0.32 mV/°C, which is indicative of tunneling [10]. This corresponds to the deviation in n = 2 current in the I_{sc} vs.V_{oc} plot [Fig 2]. Thus, once the InGaAsSb overcomes a tunneling current threshold, both material systems exhibit similar temperature dependence of V_{oc}. Lattice-matched InGaAs (E_g = 0.73 eV) and GaSb (E_g = 0.7 eV) also show temperature dependences of 1.5-1.6 mV/°C, which are also independent of current level.

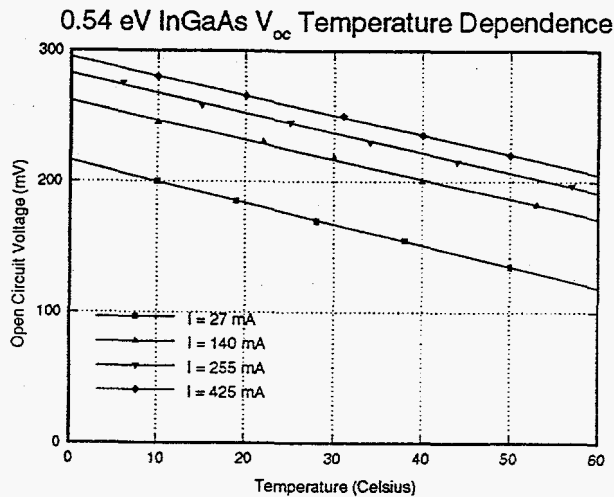## 0.54 eV InGaAs V_{oc} Temperature Dependence

Figure 3 - 0.54 eV InGaAs open circuit voltage temperature dependence.

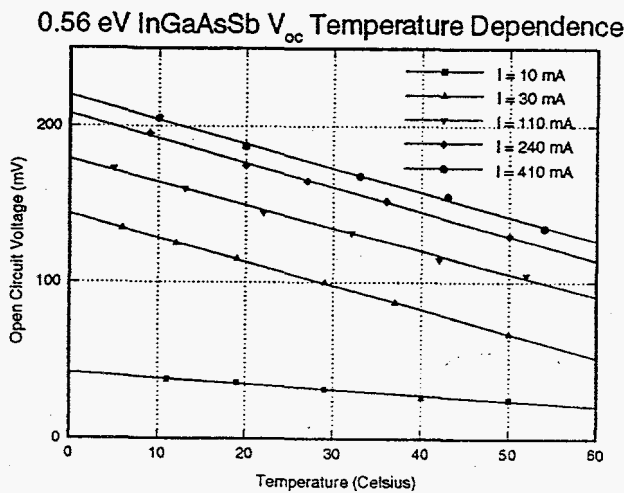## 0.56 eV InGaAsSb V_{oc} Temperature Dependence

Figure 4 - 0.56 eV InGaAsSb open circuit voltage temperature dependence.

Fill-factors of 60-65% have been achieved on both InGaAs and InGaAsSb devices at current densities of 5A/cm^2 operating at room temperature. This is within 10% of the theoretical maximum, assuming radiative limited dark current and zero series resistance [11]. In addition to conventional series resistance components (eg., gridlines, contact resistance, etc.), all semiconductor heterojunction barriers that may also contribute to unwanted series resistance must be minimized. This is particularly troublesome for the InGaAsSb:GaSb interface [12].

Finally, the performance of these devices was compared to other published data. Shown in Fig. 5 is a comparison of InGaAs dark current as a function of bandgap in comparison with the radiative dark current limit [11]. Included in this chart are published InGaAs detector (reverse-bias current), and thermophotovoltaic (voltaic dark current) data. Here, the detector dark currents are typically measured at 5-10 mV reverse bias, while TPV dark currents are extracted from I_{sc} vs. V_{oc} data. The most extensively studied InGaAs composition is lattice matched to InP substrates (E_g = 0.73 eV). Figure 5 suggests that the voltaic dark current is 1-2 orders of magnitude smaller than the reverse-bias dark-current measurements in optimized 0.73 eV devices (this has been confirmed in separate measurements). This is due to the predominance of R-G dominated dark current, which typically dominates in reverse bias. As the bandgap decreases, the TPV dark current is no longer 1-2 orders of magnitude lower than the detector data. This suggests further improvements in InGaAs TPV devices are possible by reduction of misfit dislocation defects.
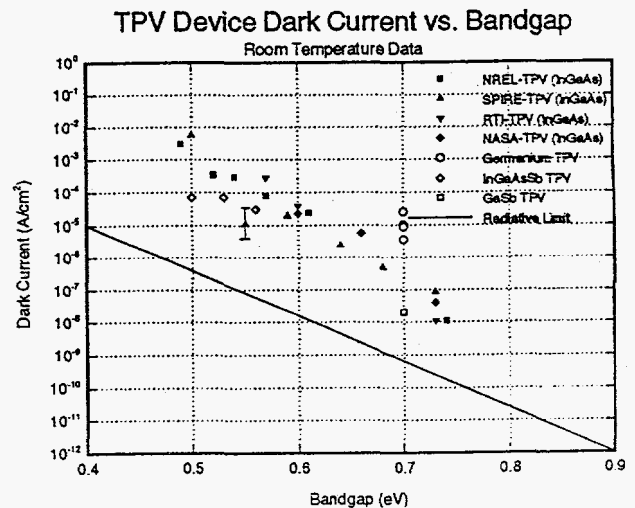
TPV Device Dark Current vs. Bandgap

Figure 5 - Comparison of published InGaAs room temperature dark currents versus bandgap.

Figure 6 illustrates a comparison of InGaAs and InGaAsSb TPV voltaic dark current versus bandgap at room temperature. Also included in this data for completeness are published results for GaSb and Ge TPV devices. Dark currents were calculated from illuminated I-V data assuming n = 1 ideality factor.
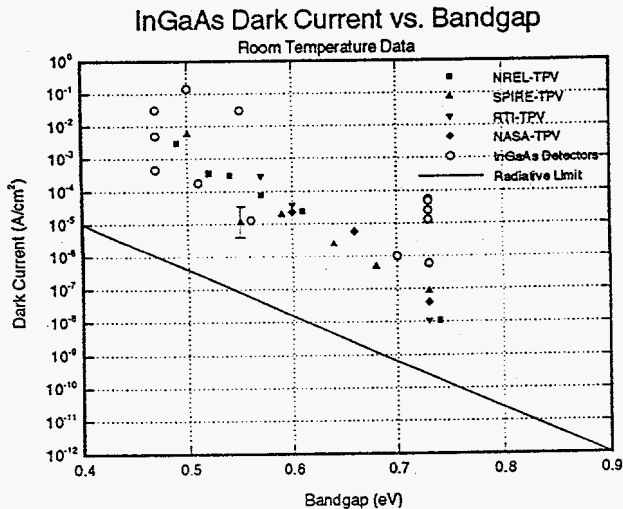

Figure 6 - Comparison of InGaAs and InGaAsSb room temperature voltaic dark current versus bandgap.

CONCLUSIONS

Currently, InGaAs lattice-mismatched devices offer superior performance in comparison to InGaAsSb lattice-matched devices, due to the former's long-term development for numerous optoelectronic applications. However, lattice-matched antimony-based quaternaries offer numerous potential advantages. Both devices exhibit similar temperature dependence of the open circuit voltage. The predominance of n > 1 dark current in InGaAsSb devices suggest further improvement in material and/or surface quality are required before the potential advantages of this material system are realized.

ACKNOWLEDGMENTS

REFERENCES

[1] 1st NREL Conference on the Thermophotovoltaic Generation of Electricity, Copper Mtn., CO, AIP Conf. Proc. **321** (1994).

[2] 2nd NREL Conference on the Thermophotovoltaic Generation of Electricity, Colorado Springs, CO, AIP Conf. Proc. **358** (1995).

[3] R. Swanson, "Silicon Photovoltaic Cells in TPV Conversion," EPRI Research Project ER-1272, 1979.

[4] P. Bhattacharya, Ed., Properties of Lattice Matched and Strained Indium Gallium Arsenide, INSPEC, London, 1993.

[5] T.P. Pearsall, Ed., GaInAsP Alloy Semiconductors, John Wiley and Sons, New York, 1982.

[6] H.K. Choi, G.W. Turner, and S.J. Eglash, "High Power GaInAsSb-AlGaAsSb Multiple Quantum Well Diode Lasers Emitting at 1.9 μm," IEEE Phot. Tech. Lett., 6, 1994, pp. 7-10.

[7] R.J. Menna, D.R. Capewell, R.U. Martinelli, P.K. York, and R.E. Enstrom, "3.06 μm InGaAsSb/InPSb Diode Lasers Grown by Organometallic Vapor-Phase Epitaxy," Appl. Phys. Lett., 59, 1991, pp. 2127-2129.

[8] A.G. Milnes and A.Y. Polyakov, "Gallium Antimonide Device Related Properties," Sollid-State Electronics, 36, 1993, pp. 803-818.

[9] S. Wojtczuk, P. Colter, G. Charache, and B. Campbell, "Production Data on 0.55 eV InGaAs Thermophotovoltaic Cells," Presented at 25th IEEE PVSC, 1996.

[10] S.R. Forrest, R.F. Leheny, R.E. Nahory and M.A. Pollack, "InGaAs photodiodes with dark current Limited by Generation-Recombination and Tunneling," Appl. Phys. Lett., 37, 1980, pp. 322-325.

[11] C.H. Henry, "Limiting Efficiencies of Ideal Single and Multiple Energy Gap Terrestrial Solar Cells," Jl. Appl. Phys., 51, 1980, pp. 4494-4500.

[12] M.P. Mikhailova and A.N. Titkov, "Type II Heterojunctions in the GaInAsSb/GaSb System," Semicond. Sci. Technol., 9, 1994, 1279-1295.